REVIEW OF AERONAUTICAL FATIGUE INVESTIGATIONS IN JAPAN DURING THE PERIOD JUNE 1999 TO JUNE 2001

Edited by

Akira Kobayashi
Science University of Tokyo

and

Hiroyuki Terada
National Aerospace Laboratory

For Presentation at the 27th Conference of
the International Committee on Aeronautical Fatigue

Toulouse, France, June 26, 2001

CONTENTS

12.1 INTRODUCTION

A. Kobayashi, National Delegate

The present national review reports aeronautical fatigue activities in Japan during 1999 to 2001. The very review is due to contributions by Aeronautical Fatigue Research Committee members of Japan Society for Aeronautical and Space Sciences, especially to the key members affiliated with the following:

National Aerospace Laboratory (NAL)
Third Research Center, Technical Research and Development Institute (TRDI), Japan Defense Agency (JDA)
Aircraft Accident Investigation Commission
Mitsubishi Heavy Industries, Ltd. (MHI)
Kawasaki Heavy Industries, Ltd. (KHI)
Fuji Heavy Industries, Ltd. (FHI)
Japan Aircraft Development Corporation (JADC)
All Nippon Airways (ANA)
University of Tokyo
Kyushu University
Science University of Tokyo
Tokyo Metropolitan University
Shonan Institute of Technology
University of Electro-Communications
University of Shiga Prefecture

The above-mentioned members are greatly appreciated for their concentrated endeavor to achieve such a fruitful review. Mr. Tadao Kamiyama, former National Delegate of Japan, is acknowledged for his everlasting encouragement during the course of compilation of the present review. Dr. Toshiyuki Shimokawa, now Professor of Tokyo Metropolitan Institute of Technology, is also acknowledged for his long-time contributions as a co-compiler of the national reviews.

.

12.2 METALS

12.2.1 Effect of Fibrous Structures on Fatigue Strength of 13-8Mo Stainless Steel

A. Sakabe and N. Ando, Fuji Heavy Industries, Ltd. (FHI), e-mail:SakabeA@uae.subaru-fhi.co.jp

As for PH13-8Mo stainless steel (AMS5629, UNS S 13800), which was precipitation heat-treated and machined, indications are sometimes detected by magnetic particle inspection, even though cracks really did not exist. Figure 12..1 shows the result of magnetic particle inspection. This phenomenon is also confirmed in 15-5PH stainless steel (AMS5862, UNS S 15500).
These indications are observed by magnetic flux leakage from fibrous structures (retained austenite; Figure 12.2 shows these structures), which is caused by segregation of materials. Fatigue tests were conducted to study the effect of these structures on strength properties.

Experiment
Two steel manufacturers' materials were used in the present tests, Lot A (3 3/4" dia. bar) was made by Japanese manufacturer and Lot B (2" dia. bar) was made by United States manufacturer. These materials heat-treated in the H1000 condition have fibrous structures in the longitudinal direction. Smooth (Kt=1.0) specimens were machined and rotating beam fatigue tests were conducted for both lots. Tests data were compared with the standard property of 13-8Mo stainless steel without fibrous structures.

Experimental Results
Figure 12.3 shows the result of rotating beam fatigue tests. There was no effect of fibrous structure on the test results in both lots. However, the very phenomenon needs to judge whether the indication of magnetic particle inspection is due to real crack or fibrous structure. This results in the increase in

cost and delay of schedule. Accordingly, fibrous structures are eliminated by means of additional requirements on the material specification at present.

12.2.2 Cast Evacuation Door -Structural Strength Test-

H. Sashikuma, Y. Mizusaki and H. Kishi, Kawasaki Heavy Industries, Ltd. (KHI)
e-mail: sashikuma_h@khi.co.jp

It is expected that the casting technology leads to the reduction of cost and weight The present study was carried out to apply casting technology to the main structures of evacuation doors for a transport airplane.

Design and Manufacturing

The design loads are defined as follows; a static pressure 18.2psi (ULT), a fatigue pressure 8.6psi x 93,000 cycles, and a fail safe pressure 10.3psi. Selected material is aluminum D357-T6, which has excellent casting characteristics and provides high strength together with good toughness, and excellent corrosion resistance. Figure.12.4 shows one piece cast evacuation door structure, whose length, width and depth are 33, 22 and 5 inches, respectively. FEM internal load analysis and strength analysis have been conducted.

Test

Structural strength tests - static, fatigue, and fail safe tests - were conducted for a prototype door structure with skin. Figure 12.5 shows the test setup. A good agreement was obtained between the results of the analysis and the tests on stresses, displacements, and supporting reaction forces.

Conclusion

The cast evacuation door structure was proved to withstand the design loads and it was confirmed that this casting design and manufacturing process are enable to reduce weight and cost compared with traditional built-up design.

12.2.3 Component Fatigue Tests for New Small Observation Helicopter (OH-1)

Shirou Miyake and Shinichirou Takanashi, 3rd RC, T.R.D.I., Defense Agency
e-mail: shirouz@jda-trdi.go.jp

The fatigue strength test of the main rotor hub, the main rotor blade and the tail rotor hub for OH-1 were carried out until April 1999. And the torsion element for the main rotor system was tested to evaluate the extension of the service life and the test was completed in August 1999. Figure 12.6 shows the main rotor system and the test of the torsion element is outlined below.

Fig.12.7 shows an overview of the torsion element. In order to change each load according to the angle of rotation, the force on the torsion element is broken down into (1) centrifugal force caused by rotation, (2) flapping force due to the dynamic lift generated, (3) torque force due to the inertia force of rotation and (4) lead lag force due to rotation. These forces act with a cyclic motion while the rotor makes one turn. To consistently apply this cyclic motion to the specimen, the point of application and the direction of application of the load must be set. Fig.12.8 shows an outline of the load application setup. Each load of (1) to (4) is applied by the electro-hydraulic servo actuator due to the computer control.

Each of the four actuators in Figure 12.8 loads with a quarter of the centrifugal load respectively. Also the actuators (a) and (b) alternatively load the flapping load and the actuators (c) and (d) also alternatively load the lead lag load by superimposing with the centrifugal loads.

12.3 COMPOSITES

12.3.1 Low Cycle Fatigue Behavior of Symmetric Angle-Ply Laminates

K. Kunoo, Kyushu University

We carried out cyclic zero-tension tests for symmetric angle-ply laminated specimens in order to investigate the low cycle fatigue behavior of graphite/epoxy and graphite/PEEK composites. The

stacking sequences of laminates were [+ /-]$_{4s}$ (Distributed Ply) and [+ $_4$/- $_4$]$_s$ (Blocked Ply), where was 30 degree or 45 degree. We obtained stress-strain curves of specimens under cyclic loadings by means of an extensometer. A mechanical ratcheting, which means progressive increase in strain at each cycle, was observed on the cyclic stress-strain curves. Comparing the stress-strain curve of static tensile test with one of cyclic zero-tension test, we made the assumption that the fatigue failure occurred when the ratcheting strain by cyclic loadings reached the static failure strain. Results of an ultrasonic scanning test revealed that the distributed ply specimens differed from the blocked ply ones in an internal fatigue damage progress. Moreover, we pointed out the difference of failure surface between static failure and fatigue failure.

Specimen and Experimental Procedure
Graphite/PEEK specimens were made from unidirectional prepreg sheets APC-2 supplied by ICI-Fiberire Co. The laminates were cut into 25mm width coupons. All specimens were tabbed by 3mm thick GFRP. An epoxy tape-type adhesive (Y-582A, Sumitomo 3M Co., Ltd.) was used to bond the tabs to both ends of the specimens. Axial and lateral strains were measured with a biaxial strain gage and extensometer in static tests. However, we measured only axial strain with an extensometer during fatigue tests because a strain gage is not reliable owing to fatigue of the strain gage itself. Loading was cyclic with a constant stress amplitude for a sine load history at a frequency of 0.02Hz and at stress ratio R less than 0.02.

Experimental Results
Stress and strain were measured continuously until twentieth cycle and then every fiftieth cycle until the collapse of the specimen. Figure 12.9 shows the stress-strain diagram of static and fatigue test for Graphite/PEEK $[+30/-30]_{4s}$. All tests were performed at room temperature. Figure 12.10 shows the distribution of the total strains to failure in static tests and fatigue tests. Static failure strains scatter ranging from 3.22% to 4.66%. Almost all the fatigue failure strains scatter in range of static failure strains except for stress amplitude of 70%. In particular, the total stains of stress amplitude of 75% agree with the average of static failure strains of 3.9% in spite of the fact that the fatigue strength of two specimens at stress amplitude 75% is very different (N_f = 71 and 181). This result implies that a total strain can be one of parameters to estimate a fatigue strength under high stress amplitude (more than 75% of the ultimate strength).

12.3.2 Residual Strength of PETI-5 With Notched Crack Under Tensile Loading

H. Tamura, Japan Aircraft Development Corporation (JADC), and S. Shirahama, Mitsubishi Heavy Industries, Ltd. (MHI)

It is crucial to estimate the residual strength of damaged composite structure in order to realize the aggressive application of composite to the primary structure of commercial airplane. Several theoretical or semi-empirical prediction methods have been introduced for estimation of residual strength of damaged composite structures. J. W. Mar and K. Y. Lin proposed the semi-empirical theory, namely “Mar-Lin method”, which was based on the linear elastic fracture mechanics as applied to homogeneous materials. Component testing was carried out to correlate the parameters that affect residual strength of damaged composite structures and the coefficients in the Mar-Lin equation. The present work was done by Mitsubishi Heavy Industries Ltd. (MHI) under the contract with Japan Aircraft Development Corporation (JADC).

Mar-Lin Method
Mar-Lin method predicts the residual strength of damaged composite by the equation

$$\sigma_N = Hc / (2a)^n \qquad (1)$$

where “a” is half crack length, Hc is referred as fracture toughness of composite and “n” is the order of singularity of a crack, of which tip is at the interface of two different materials. Hc for the laid-up composite is considered to be independent of a crack size just like for homogeneous materials, but to be dependent on lay-up patterns while Hc for homogeneous materials is constant. The “n” in turn is supposed to be independent of lay-up patterns but dependent upon a crack size.

Since the 90° ply layer in which fiber runs parallel to the crack has negligible effect to arrest the

crack propagation, it can be assumed that only the amount of 0° and 45° plies can be the parameters to determine Hc. Thus Hc can be estimated by

$$Hc = k0\,(p0)^{n0} + k45\,(p45)^{n45} \quad (2)$$

where p0 and p45 are percent of 0° ply and 45° ply respectively. The following values are proposed for MR-50K/PETI-5 material.

$$k0 = 36.7, \quad n0 = 0.55$$
$$k45 = 11.0, \quad n45 = 0.55 \quad (3)$$

The order of singularity increases as the notch size grows. For the material in the present study, the coefficient "n" can be written as follows.

$$n = 0.23\,(1 - \log_{2a}(25.4)) \quad (\text{for } a < 12.7 \text{ mm}) \quad (4)$$
$$n = 0.56\,(1 - \log_{2a}(25.4)) \quad (\text{for } a >= 12.7 \text{ mm}) \quad (5)$$

Component Testing

The damaged specimens which have a notched through crack in the center of the panel were loaded in tension to obtain residual strength data of the panel. Each specimen has different configurations with various parameters such as lay-up patterns, crack length (2a) and panel width (W) while the ratio W/(2a) is kept constant (4.0).

Validation of the Equation

A modified Mar-Lin method to predict residual strength of damaged PETI-5 composite panels was obtained. Using this modified Mar-Lin method, residual strength of damaged PETI-5 composite panels for area where test data are not available, can be predicted. Figure 12.11 shows the comparison of the residual strength of damaged composite specimen derived from the equation (1) through (5) and the data obtained by the test conducted by MHI.

12.3.3 Microscopic Damage Extension in Carbon/Bismaleimide Cross-ply Laminates Under Fatigue Loading

S. Kobayashi, Tokyo Metropolitan University, koba@ecomp.metro-u.ac.jp, N. Takeda, The University of Tokyo, S. Ogihara and A. Kobayashi, Science University of Tokyo

The objective of the present study is to investigate the microscopic damage extension in carbon fiber reinforced bismaleimide composites, one of the current candidate structural materials for a next generation supersonic transport (SST). Three type cross-ply laminates were tested to discuss the effect of 90° ply thickness on the transverse cracking behavior.

Experiment

A material system used is carbon fiber (G40-800) reinforced bismaleimide (5260). Bismaleimide is a heat resistant polymer, which is considered to be a potential material system for future SST structures. Laminate configurations tested were three types of cross-ply laminates, $[0/90_2/0]$, $[0_2/90_3/0_2]$ and $[0_2/90_4/0_2]$ to study the effect of 90° ply thickness on the transverse cracking behavior. The specimen size was 150mm long and 25mm wide. GFRP tabs were glued on the specimens resulted in the specimen gauge length of 80mm. Free edges of specimens were polished for the observation using an optical microscope. All the specimens were stored in a desiccator to avoid the moisture effects.

Tension-tension fatigue tests were conducted using an electro-hydraulic testing machine. All tests were run at the stress ratio, R=0, a frequency of 5Hz and room temperature and with a sinusoidal waveform under the load control condition. The maximum stress levels were selected to correspond to the laminate strains of 0.5% and 0.6% for each laminate. During the test, the testing machine was periodically stopped, and the edges of the specimens were observed by an optical microscope directly. The specimens were also observed by a soft X-ray radiography to detect transverse crack extension in the width direction. The number of transverse cracks per unit observed length was defined as the transverse crack density.

Experimental Results

Figure 12.12 shows the relation between the transverse crack density in 90° plies observed at the free edges and the number of cycles. In the $[0/90_2/0]$ laminate, no transverse cracks were observed until

n=1,000,000 (n is the number of cycles) at 0.5% strain. Transverse crack onset cycles were the smallest in the $[0_2/90_3/0_2]$ laminate under the same maximum stress level, because the thermal residual stress was the largest in $[0_2/90_3/0_2]$. Transverse crack density was also the largest at the same cycle in $[0_2/90_3/0_2]$. Comparing $[0/90_2/0]$ and $[0_2/90_4/0_2]$ laminates in which the thermal residual stresses in 90° ply were expected to be the same, transverse crack onset cycles were larger in the $[0/90_2/0]$ laminates with thinner 90° ply thickness. This may be explained by the energy release rate analysis. From the X-ray observation, it was found that transverse cracks initiated at the free edges and grew in the width direction.

12.3.4 Application of a Compliance Method to Fatigue Crack Growth Analysis of GLARE3 Fiber/Metal Laminates

T. Takamatsu, University of Shiga Prefecture, T. Shimokawa, National Aerospace Laboratory, and T. Matsumura, University of Electro-Communications

The objectives of the present study were to investigate the effectiveness of a compliance method for analyzing the fatigue crack growth of GLARE3 fiber/metal laminates, and to ascertain the influence of specimen thickness, notch length, and fiber orientation upon fatigue crack growth. The materials tested were GLARE3-5/4 and GLARE3-3/2. Centrally notched specimens with two kinds of notch length and two kinds of fiber orientation were fatigue tested under constant amplitude loading. The experimental stress intensity factors, K_{exp}, for the 2024-T3 aluminum-alloy layers of a GLARE3 were obtained from the relationship between the crack length and the specimen compliance. The test results clarified that $da/dN - \Delta K_{exp}$ relationships are roughly independent of maximum stress level, specimen thickness, notch length, and fiber orientations and that the compliance method is effective for analyzing fatigue crack growth in GLARE3 laminates.

12.3.5 Axial Fatigue Strength of Open-hole Specimens of T800H/PMR-15 Carbon/Polyimide Composite at Room and High Temperatures

T. Shimokawa, Y. Kakuta, National Aerospace Laboratory(NAL),
T. Tanimoto, and J. Morishige, Shonan Institute of Technology

A joint research program was conducted to investigate fatigue properties of a carbon/polyimide composite nominated for the primary and secondary structures of the HOPE-X, an unmanned small space shuttle. The objective is to investigate the axial fatigue strength of open-hole specimens at room and high temperatures.

The laminate tested is made of T800H/PMR-15 carbon/polyimide system (ICI Fiberite). Figure 12.13 indicates the specimen configuration. Open-hole specimens were machined from the panels with a quasi-isotropic stacking sequence, 32 plies $(45/0/-45/90)_{4S}$. The nominal thickness of the prepreg system is 0.134 mm and that of the laminate 4.29 mm.

Axial fatigue tests were conducted in laboratory at room temperature (RT) and in an air-circulating oven at 260°C. This high temperature is provisionally fixed as the upper limit of this material under mechanical loading conditions in use for the space shuttle structures. An electronic servo-hydraulic fatigue-testing machine was used under the constant amplitude loading of sinusoidal waves with a frequency of 10 Hz. Three kinds of stress ratio (R=minimum stress/maximum stress) were selected; 0.1 (tension-tension), 10 (compression-compression), and -1 (fully reversed). Prior to fatigue testing, specimens were kept in a thermo-hygrostat for 48 hours in order to control the moisture content of specimens. The air in the thermo-hygrostat was adjusted to 23°C and 65% relative humidity. Axial fatigue tests provided S-N relationships up to 10^6 cycles. Additionally the fatigue failure modes were investigated.

Figure 12.14 presents S-N relationships. The maximum absolute stress as the ordinate indicates the maximum stress for fatigue tests of R=0.1 and -1 and the absolute values of the minimum stress for fatigue tests of R=10. A regression analysis provided approximate S-N lines in Fig. 12.14 on the basis of failure data only. When the slope of an S-N line was positive, a horizontal line represented this line. Fatigue strength reduction was evaluated at 10^5 load cycles, because most of the fatigue strength at 10^5 existed in the interpolated region of the S-N lines in Fig. 12.14.

Major test results obtained and conclusions are as follows:
(1) Horizontal *S-N* lines appeared for the combinations of (R=0.1, RT), (R=0.1, 260°C), and (R=10, 260°C). In other cases the slope of other *S-N* lines was negative and very small. Therefore, the scatter of fatigue life was considered very large.
(2) Two *S-N* lines at room temperature for R=0.1 and 10 passed through the tensile and compressive static strengths. Both *S-N* lines at 260°C for R=0.1 and 10 were horizontal and lower than those at room temperature. However, more test results should be collected in order to conclude the two *S-N* lines at 260°C horizontal.
(3) When comparing fatigue strength at $N=10^5$ cycles, fatigue strength at 260°C is 18 % lower than that at RT for R=0.1, 7.5 % lower for R=10, and 27% lower for R=-1. These reductions indicate the effect of high temperature.
(4) In fully reversed fatigue tests, R=-1, only compressive stress amplitude is effective for reducing fatigue strength at RT. Most fatigue strength reduction is provided by compressive stress amplitude, but tensile stress amplitude partly contributes to fatigue strength degradation at 260°C.
The failure modes are similar at RT and 260°C in the same stress ratios. An axial splitting failure mode and fiber pull-out appeared for R=0.1; however, that of a rhombus shape (in side view), caused primarily by delamination buckling, appeared for R=10, and for the combination of R=-1 and RT. The failure mode for the combination of R=-1 and 260°C showed a mixed mode with those seen for R=0.1 and 10, although it is close to that for R=0.1.

12.3.6 Effects of Thermal Cycling on Degradation of High-Temperature Polymer Composite Materials for the Next-Generation SST Structures*

T. Shimokawa and H. Katoh, National Aerospace Laboratory(NAL)

The structures of the next-generation supersonic transport (SST) require long term durability of structural materials under a variety of conditions involving temperature, loadings, and fluids, not only in constant states but also in cyclic fluctuations. Moreover, the structural weight must be drastically reduced to ensure commercial success. This requirement demands extensive use of high-temperature polymer matrix composite materials.

National Aerospace Laboratory (NAL) is carrying out joint research programs with three major aircraft industries in Japan and Japan Aircraft Development Corporation (JADC) to evaluate the long-term durability of high-temperature polymer matrix composite materials nominated for use in SST. As one of the joint research programs, the present study investigated the effect of thermal cycling for an SST supposed to encounter in service on the degradation of the composite materials.

Thermal cycling was designed to be one cycle from RT (room temperature) to -54°C (15 minutes hold), then to 149 or 177°C (15 minutes hold), and back to RT, elapsing approximately 38 minutes. Figure 12.15 presents an example of test thermal cycle measured. Thermal cycling tests were conducted up to 10,000 cycles on three kinds of carbon fiber/high-temperature polymeric composite materials, i.e. IM7/PIXA, IM7/K3B, and G40-800/5260. After thermal cycling tests, the number of micro cracks initiated on the sectional surface of the laminates was counted by optical microscope observation. Static mechanical tests provided the open-hole compressive strength before and after thermal cycles. In addition, a simple FEM model using the basic data of T800H/PMR-15 carbon/polyimide composite material estimated the thermal stress produced in the laminate.

Major results obtained are as follows:
(1) Figure 12.16 indicates the number of micro cracks initiated per 10mm×thickness as a function of thermal cycles. The number of micro cracks initiated was different with the materials, as shown in this figure.
(2) Figure 12.17 presents the open-hole compressive strength before and after thermal cycles. Thermal cycles and initiation of micro cracks did not affect the open-hole compressive strength within the results in Fig. 12.17.
(3) The calculated stress level induced by one thermal-cycle with a temperature range of 231°C was under the limit level of crack initiation; however, if the fatigue is considered, this thermal-stress cycle was very severe.

* T. Shimokawa, H. Katoh, Y. Hamaguchi, S. Sanbongi, H. Mizuno, H. Nakamura, R. Asagumo, and H. Tamura, "Effects of Thermal Cycling on Degradation of High-Temperature Polymer Composite Materials for the Next-Generation SST Structures," Proceedings of the 9th United States - Japan Conference on Composite Materials, Mishima, Japan Society for Composite Materials and American Society for Composites, 2000, pp. 355-362.

12.3.7 Fatigue Tests and Improvement of Bearingless Rotor for Medium-Sized Helicopter

J. Takaki, Fuji Heavy Industries LTD.(FHI)

Fuji Heavy Industries LTD. is developing the new main rotor system, Fuji Bearingless Rotor, FBR, for medium-sized helicopters. The FBR is a soft-in-plane bearingless rotor system which has four composite blades and composite hub structure. The FBR can provide higher airspeed, larger flight range, more structural reliability and maintainability rather than the existing rotor, even though low noise and low vibration can be achieved.

The FBR shown in Figure 12.18, has 46 feet diameter and 14.5inch chord. The rotor consists of four GFRP rotor blades, two GFRP flexbeams as the hub structure, eight lead-lag damper assemblies, and four CFRP pitch sleeves. The main rotor blade is attached to the flexbeam with a bolt and an expandable pin and can be folded to save storage space. Two flexbeams are stacked and bolted to the mast flange to form the four bladed configuration. The pitch sleeve has the function to effect blade pitch change and made of CFRP composite material to realize high torsional rigidity. The prototype main rotor system has been demonstrated during flight tests in 1996, as shown in Figure 12.19. Flight tests were completed successfully and showed the applicability of our design.

The flexbeam is the main structure for blade retention and due to its flexibility, replaces the mechanical rotor hinges. This structure is applied the huge centrifugal force and the cyclic deformation due to flapping and feathering motion during rotation of rotor. The flexbeam should be designed to allow numerous cycles of large elastic deformation withstanding the huge centrifugal force.

The structural substantiation was conducted according to FAA Far Part 29 and FAA Advisory Circular 20-107A for composite structure. The Building Block Approach, Figure 12.20, was used to substantiate the composite structures. The tests of coupon/ element/ sub-component and the component test were conducted to show the static and fatigue strength of the composite structures. The coupon, element and sub-component tests were conducted to establish the material allowable values and design values to design including the possible degradation of environmental exposure. The component tests were performed to demonstrate the static and fatigue strength of the actual composite structure with the elevated load level and to establish the S-N data to determine the working curves to substantiate the fatigue strength of components during the flight test. All composite components were evaluated by fatigue tolerance evaluation (including tolerance to flaws) or fail-safe (residual strength after flaw growth) evaluation.

After the flight tests of the prototype FBR, the development are following to design the production FBR. The improved flexbeam was designed and manufactured. The fatigue test results, Figure 12.21, show the improved flexbeam can satisfy the fatigue design target for production.

12.4 SHORT CRACK

12.4.1 Propagation of a Short Crack in Aircraft Lap Joints

P. A. Dybskiy, H. Terada, and T. Okada, National Aerospace Laboratory (NAL)

The idea to describe whole fatigue life as solely crack propagation phenomenon has showed to be able to provide reliable predictions for airframe applications. In the present study simplified variation of methodology proposed by J.C. Newman was used to simulate results which were observed during the fatigue test of three barrel articles subjected to constant amplitude pressure, pressure/bending, and pressure/bending/torsion load with maximum pressure of 0.125 MPa, min/max pressure ratio R=0.05, upward/downward lateral force (±1000kgf and ±2000kgf), and synchronized with the main pressure cycle. The main efforts were placed at the local stress variation

in the zone surrounding countersunk hole subjected to complex loading conditions caused by biaxial tension of skin, rivet clamping and bearing force, eccentricity of load transferred by lap joint, and friction between components of the joint.

Typical corner crack configuration at the countersunk hole edge captured by SEM is given in Figure 12.22. FEM model adopted for FEM analysis is shown in Figure 12.23. Load conditions are as follows: a main hoop tension 90 MPa, bending deflections 0, 0.05, and 0.1mm; a lateral axial tension, 16, 40, and 62 MPa; the load transfer factor 0.2, 0.3, and 0.4; total clamping forces, 0, 200, and 400 N; a friction coefficient 0, 0.15, and 0.30. The followings were concluded from FEM of rivet joint:

1) Location of point of maximum stress concentration with reasonable degree of accuracy can be assumed at 90 degree along the hole circumference,
2) Friction has a small effect on the stress concentration (about 3% for 100% variation in *Kfr*),
3) Local bending and load transfer factor have the most significant effect (up to 15%) on the stress concentration,
4) Lateral tension is able to cause 10% variation of maximum stress level,
5) Rivet squeezing changes the initial tensile stress level within range of 5% to 8% of maximum stress for given applied loads.

To estimate propagation of a crack through the rivet hole chamfer five crack front locations were selected starting from small crack of the order of ten microns at the rivet hole knife-edge and ending with through-the-skin-thickness oblique crack. All cracks are circular. The boundary correction factors F_t,F_b,and F_w obtained by A. Rahman, Bakuckas J. G. Jr. et al. were used for all other crack locations to get value of K_I. Stress intensity factors for tensile and wedge load were derived from factors F_t, and F_w using the superposition principle. Concerning the crack growth law a piece-wise power function approximation of the baseline proposed by J.C. Newman et al. was used in the study. Comparing experimental results and theoretical estimates it can be concluded that the cases of 40 micron initial crack with the plastic closure or 6 micron initial crack without closure provide the best fit for most realistic value of LT=0.3.

Several concerns were related to the K solutions used in the study especially in the small crack range, viz. what K-solution should be used to cover variety of small crack front shapes; how to incorporate into the prediction methodology the role of microstructure as initial crack size (6-10 microns) became smaller against relatively big grain sizes of aluminum alloys (20-50 microns); also, the effect of plasticity needs proper and effective treatment in the range of small cracks.

12.5 STRESS MEASUREMENT

12.5.1 Stress and Crack Measurement of Fastener Joint by Thermography

T. Okada, H. Terada and P. A. Dybskiy, National Aerospace Laboratory (NAL)

As fatigue cracks generally start from the fastener holes, the fuselage lap joint is one of the most critical locations in view of the durability of aircraft structures. However, as the strain distribution near a rivet hole changes steeply, its measurement by strain gauge is not always valid because of its large gauge length. On the other hand, modeling of contact problems of mating plates and also between rivet hole and rivet shank are so complicated that numerical calculation might not lead to the realistic results. Therefore in the present study thermography was used to measure the stress distribution around a rivet hole. It can measure the sum of principal stresses under cyclic load and provides whole stress distribution on the surface of the specimen.

Configuration of the specimen provided for the test is shown in Fig. 12.24. The diameter of countersunk rivet head and rivet shank is 5.5mm and 3.2mm, respectively. Sheet material is Al-clad 2024-T3. The load range, the stress ratio and the loading frequency were 21.8kN, 0.15 and 5Hz, respectively. To obtain high emissivity (0.95), the black paint was sprayed on the surface of the specimen.

The stress distribution and the dissipated energy image at the rivet hole of number 4 to 8 at 192,500

loading cycles are shown in Fig. 12.25 and Fig. 12.26. From Figure 12.25, no stress decrease above the top row of No. 8 rivet is observed, whereas a remarkable stress decrease is observed above another rivet holes. From Figure 12.26, both sides of No. 5 and No. 6 rivets indicate high energy dissipation. Both sides of rivet holes of No. 4 and No. 7 rivets also show energy dissipation. By the visual inspection, through cracks were observed at both sides of rivet hole No. 5 and No. 6, and part through cracks started from both sides of rivet hole No. 4 and No. 7 were also observed after the total failure of the specimen. In conclusion, it was confirmed that the energy dissipation mode corresponded well to the fatigue crack tip, regardless of surface crack or subsurface crack.

12.6 MAINTENANCE

12.6.1 Repair Assessment Results for ANA B747 Series Airplanes

N. Wakita, T. Iwase and T. Nagasaka, All Nippon Airways(ANA)

Structure repairs applied on the pressure boundary structure (skin and bulkhead webs) may degrade as airplanes age, and at a certain time threshold close to Design Service Objective (DSO) – 20,000 cycles for B747, supplemental inspections on repairs are necessary to maintain damage tolerance. In 2000, the FAA issued a Final Rulemaking which requires operators to incorporate repair assessment guidelines for the fuselage pressure boundary into their FAA approved maintenance or inspection program.

From October, 2000 to February, 2001, ANA performed the repair assessment on 6 ANA B747 airplanes to comply with the FAA requirements. The present paper introduces general requirements and results of the repair assessment.

Requirements

All the B747 airplanes over 15,000 cycles are required to be inspected for the repair assessment program, and repairs are classified into Categories A, B and C according to their repair configuration, such as the doubler size, the fastener type, the location and others. Category A means no further action, Category B requires supplemental inspection, and Category C requires the replacement in repair.

Assessment results

We have found no category C repairs. However, total 103 repairs (87% of all the repairs) on 6 airplanes were classified as Category B, and supplemental inspections were required to these repairs. Table 12.1 shows detailed assessment results. As shown in Table 12.1, the number of repairs increases as airplanes accumulate flight cycles. Especially after 20,000 cycles, the total number of repairs increases drastically as Fig. 12.27 shows, and the calculation based on ANA present flight schedule shows about 4 repair doublers have been installed on one airplane per year after 20,000 flight cycles. Figure.12.27 also shows Category B repairs increase rapidly after 20,000 flight cycles while category A repairs exhibit a gradual increase. Fig. 12.28 shows a typical Category B repair. In this case, the length of the doubler exceeds 12 inches in the longitudinal direction, which is a limit in size and the location for Category A repairs, thus results in Category B.

Supplemental inspection

Fig. 12.29 shows an example of supplemental inspections. In this case, a HFEC (High Frequency Eddy Current) or LFEC (Low Frequency Eddy Current) inspection is required on the repair doubler along the most outer row of fasteners as shown in Fig.12.29. If HFEC inspection is selected, the access from the inside and the repetitive inspection at 12000cycle intervals are necessary. If LFEC inspection is selected, the repetitive inspection at 3,000 cycle intervals are required from the outer surface of the repair doubler.

Man –hours for repair assessment

ANA unexpectedly consumed a lot of man - hours for the assessment. Table 12.2 shows actual man-hours consumed on each airplane. ANA still has an additional 38 airplanes, and will need a total of 10,000 man-hours to accomplish the assessment on all the affected airplanes.

Further, we estimate average 400 man–hours per airplane will be necessary for supplemental

inspections, if ANA operates the airplanes for a total of 25 years.

Conclusion
1)87% of the repairs need supplemental inspections.
2)For B747, the number of repairs drastically increases after 20,000 flight cycles.
3)Consumed man–hours for the assessment are unexpectedly high, and will be an economical burden to ANA.
To date, no critical damage has been found.

12.7 AIRCRAFT ACCIDENT INVESTIGATION

12.7.1 Aircraft Accident Investigation in Japan

Atuhiko Wataki and Takumi Sato: Aircraft Accident Investigation Commission
e-mail: wataki-a25q@mlit.go.jp

As of December 31, 2000, the number of civil aircraft registered in Japan was 2,802 including 1,220 airplane (of which 647 were reciprocating engine airplane), 957 helicopters, 624 gliders including motor-gliders and 1 airship. The number of accidents occurred in Japan for past 2 years are shown in Table 12.3.

Accident due to Fatigue Failures
Table 12.4 shows the detailed classification of accident due to mechanical failures. The number in parenthesis indicates the number of the accidents caused by fatigue failure.

Two cases are described in what follows.

Case 1. fuel pipe failed by fatigue
A joint tube in PiperPA-28R-201 with a Lycoming IO-360-C1C6 engine was installed in the exit side of the fuel injector to measure both the fuel pressure and the fuel temperature for the purpose to develop the new engine. The said plane ditched offshore due to fuel exhaustion. The corner of groove of a slip ring was found to be too sharp resulting in an initiation of fatigue crack growth until fracture after about 3,000 cycles. (Figure 12.30)

Case 2. engine connecting rod failed by fatigue
During an official test flight of Beechcraft A36 with a Continental IO-520-BA engine, one engine connecting rod was suddenly broken leading to an emergency landing in a nearby rice field. After engine overhaul, about 70 striations presumably appeared recently in the fracture surface of the above-mentioned rod were found. The supposed-to-be origin of this fatigue fracture was crushed to be invisible to observe any striation there. While a small dent was found around the starting point of this fatigue fracture, therefore the very dent, maybe produced during the manufacturing process, was supposed to become an origin of the present fatigue crack growth up to fracture. Engine overhaul interval was 1,700 hours and the said engine elapsed about 565 hours. (Figure 12.31)

12.8 ICAF DOCUMENTS DISTRIBUTED BY JAPAN DURING 1999-2001

No.2223 “Goodness-of-fit tests for the type-1 extreme-value and two-parameter Weibull distributions with unknown parameters estimated by graphical plotting techniques ---Part 1: critical values,” T.Shimokawa and M.Liao
No.2224 ditto----Part 2: power study, M.Liao and T.Shimokawa
No.2225 “Effect of isothermal aging on ultimate strength of high-temperature composite materials for SST structures,” T.Shimokawa, Y.Hamaguchi, Y.Kakuta and H.Kato; T.Sanda, H.Mizuno and Y.Toi
No.2226 “Goodness-of-fit tests for type-1 extreme-value and 2-parameter Weibull distributions,” T.Shimokawa and M.Liao
No.2227 “Fatigue crack growth properties of a GLARE 3-5/4 fiber/metal laminate,” T.Takamatsu, T.Matsumura, N.Ogura, T.Shimokawa and Y.Kakuta
No.2228 “Prediction of tensile fatigue life under temperature environment for unidirectional

CFRP," Y.Miyano, M.Nakada, H.Kudoh and R.Muki
No.2229 "Effect of moisture absorption on hot/wet compressive strength of T800/PMR-15 carbon/polyimide," T.Shimokawa, Y.Hamaguchi and H.Kato
No.2230 "Evaluation of notch sensitivity of Inconel 718 at elevated temperatures," Q.Chen, N.Kawagoishi, H.Nisitani, M.Goto and E.Kondo
No.2232 "Creep-fatigue small crack propagation in a single crystal Ni-base superalloy CMSX-2 microstructural influences and environmental effects," M.Okazaki and Y.Yamazaki
No.2233 "Fatigue crack growth properties of a GLARE 3-5/4 fiber/metal laminate," T.Takamatsu, T.Matsumura, N.Ogura, T.Shimokawa and Y.Kakuta
No.2234 "Effects of thermal cycling on damage progress in interlaminar-toughened CFRP cross-ply laminates," S.Ogihara, K.Matsuo and A.Kobayashi
No.2235 "Effects of stacking sequence on microscopic fatigue damage development in quasi-isotropic CFRP laminates with interlaminar-toughened layers," S.Ogihara, N.Takeda, S.Kobayashi and A.Kobayashi
No.2241 "Evaluation of notched fatigue strength at elevated temperature by linear notch mechanics," Q.Chen, N.Kawagoishi and H.Nisitani
No.2270 "Fatigue thresholds of discontinuously reinforced aluminun alloy correlated to tensile strength," K.Tanaka et al.

ACKNOWLEDGMENTS

Dr.Shinji Ogihara, Assistant Professor of Science University of Tokyo, is greatly appreciated for his elaborate preparation shown during the course of compilation of present national review.

Table 12.1 Airplane data and the number of repair doubler

A/C No.	Delivery	Flight cycle	DSO (%)	Number of repair	Repair category			Inspection date
					A	B	C	
JA8146	Jun-80	35,328	177	29	3	26	0	Feb-01
JA8147	Feb-81	32,709	164	25	2	23	0	Oct-00
JA8153	May-81	32,151	161	36	9	27	0	Feb-01
JA8156	Jul-82	26,170	131	12	2	10	0	Nov-00
JA8159	Jal-83	29,311	147	16	0	16	0	Oct-00
JA8965	Apr-95	10,379	52	1	0	1	0	Oct-00

DSO: Design Service Objective (20,000 Flight cycles)

Table 12.2 Man –hours for assessment

A/C NO.	Access /Restore	Inspection	Total MH
JA8147	unknown	270	270
JA8156	57	127	184
JA8159	174	247	421
JA8965	41	126	167

Table 12.3 The number of accidents occurred in Japan for recent two years.

Year Kind of Aircraft	1999	2000	Total
Airplane	10	6	16
Helicopter	7	11	18
Glider/Motor Glider	5	5	10
Other(ULP etc.)	6	6	12
Total	28	28	56

Table 12.4 The number of accidents caused by mechanical failure.

Kinds of Aircraft	Cause				Total
	Airframe		Power Plant		
	1999	2000	1999	2000	
Airplane	1(1)	1	1(1)	2(2)	5(4)
Helicopter	0	1	0	0	1
Glider/Motor Glider	1	0	0	0	1
Other(ULP etc.)	0	0	0	0	0
Total	2(1)	2	1(1)	2(2)	7(4)

Note : The number in parenthesis indicates the accidents by fatigue failure.

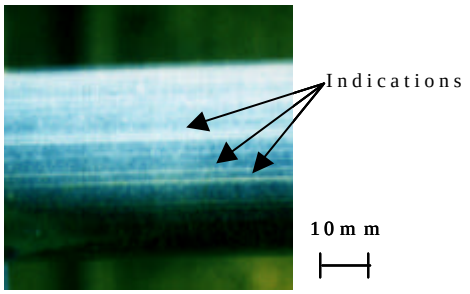

Figure 12.1 Result of magnetic particle inspection

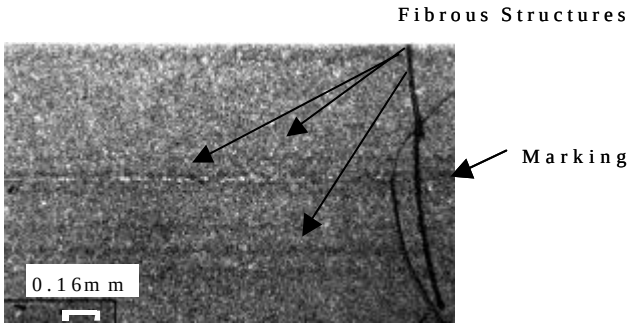

Figure 12.2 Microstructures of PH13-8Mo, (H1000). Vilella's reagent.

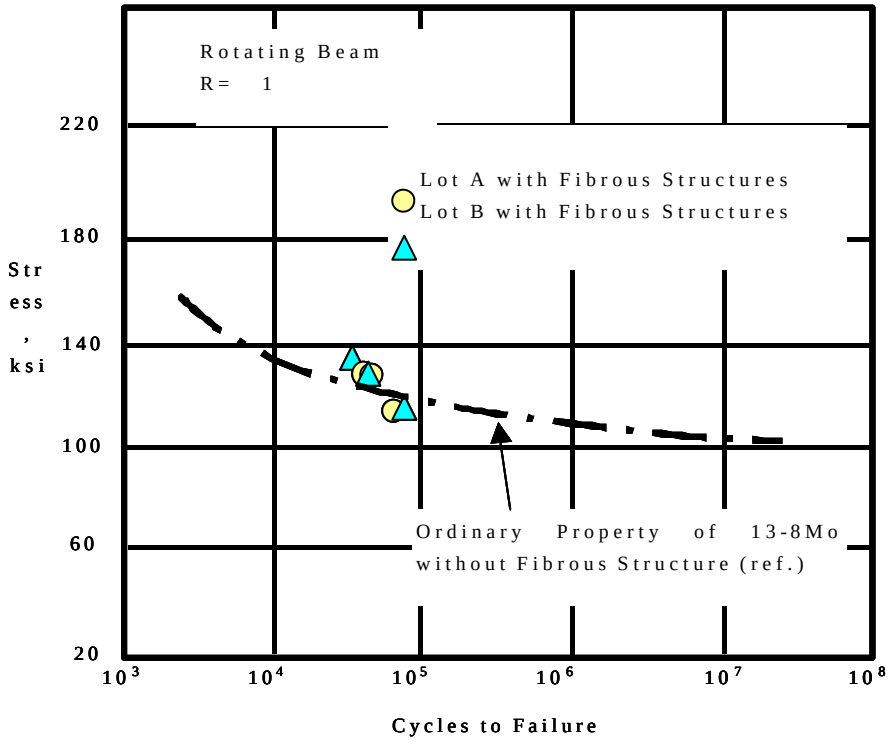

Figure 12.3 S-N curve for PH13-8Mo, bar, condition H 1000 (Kt=1.0)

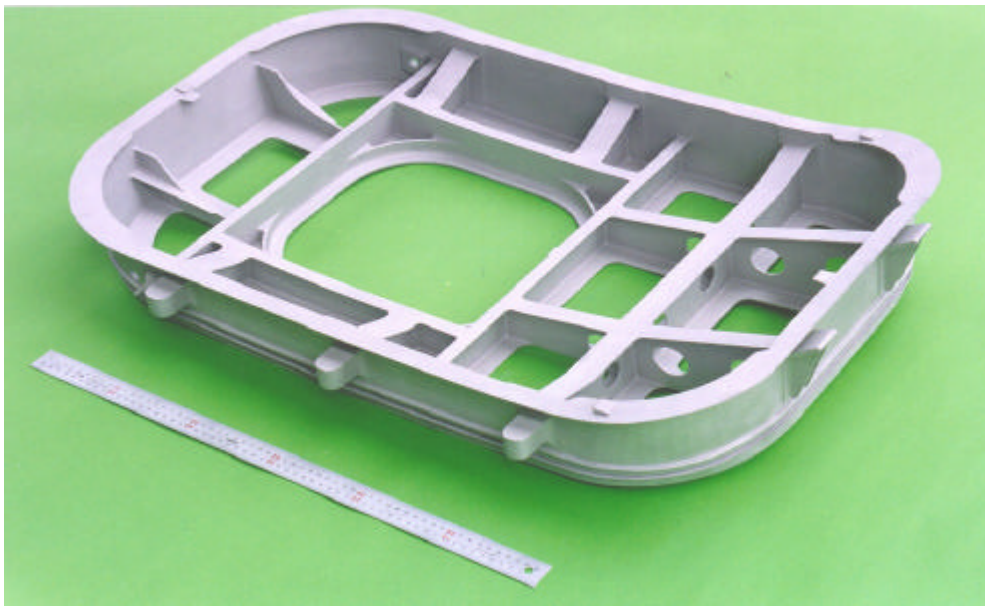

Figure 12.4 Cast evacuation door structure (inner side)

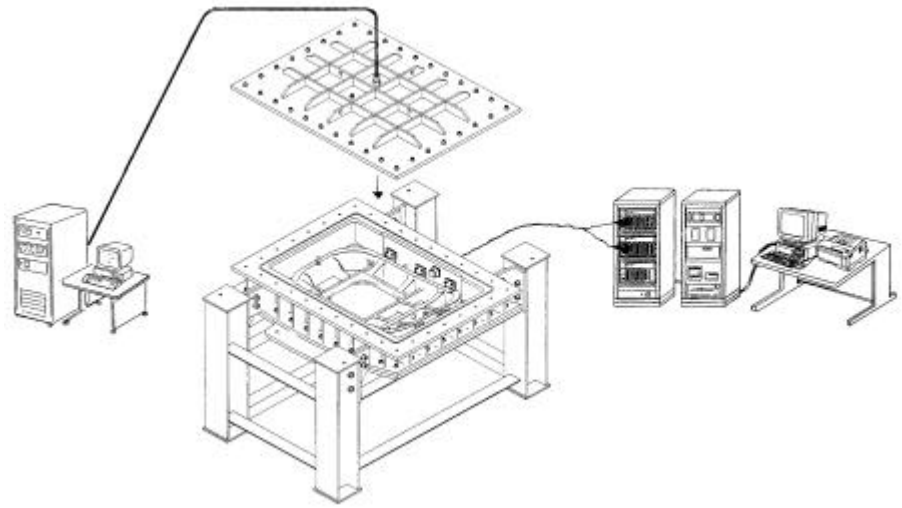

Figure 12.5 Test setup

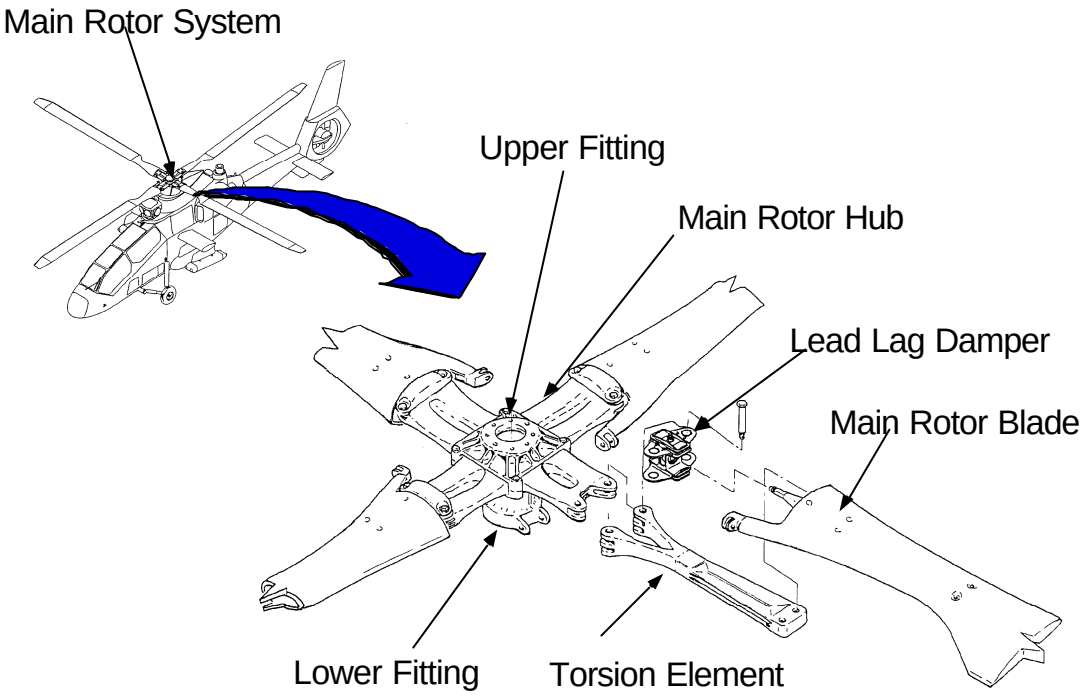

Figure 12.6 The Torsion Element of the Main Rotor System

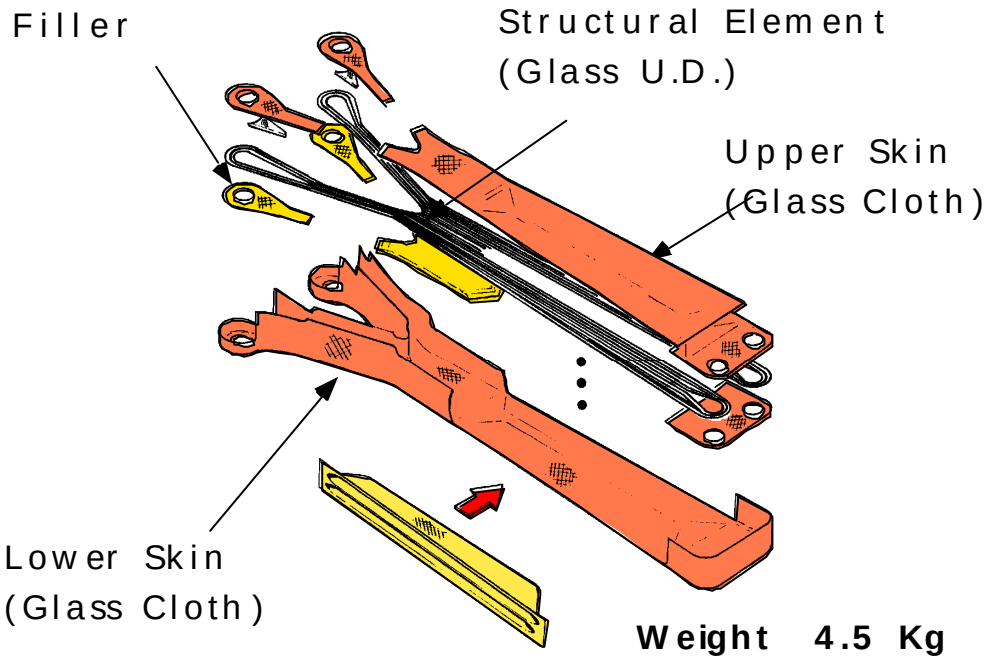

Figure 12.7 The Structure of the Torsion Element

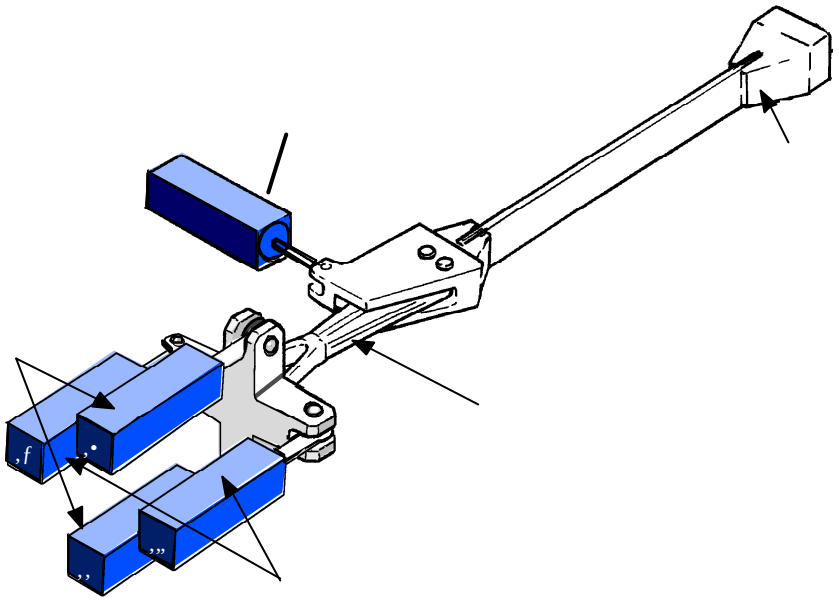

Figure 12.8 The Torsion Element Test Setup

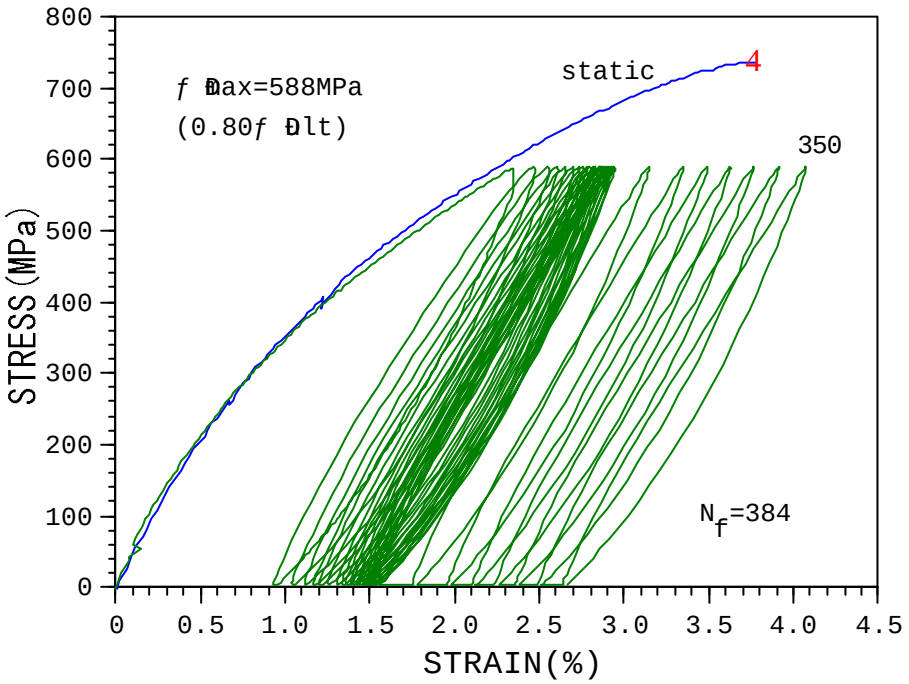

Figure 12.9 Stress-Strain Diagram of Static and Fatigue Test for $[+30/-30]_{4s}$

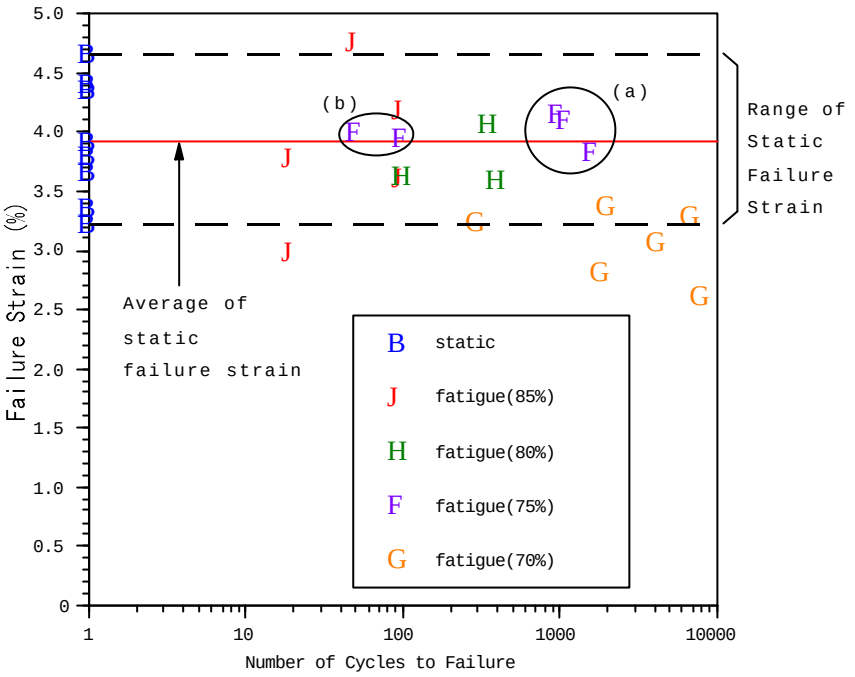

Figure 12.10 Comparison between Static and Fatigue Failure Strain

Figure 12.11 Residual strength comparison between analytical prediction and test data

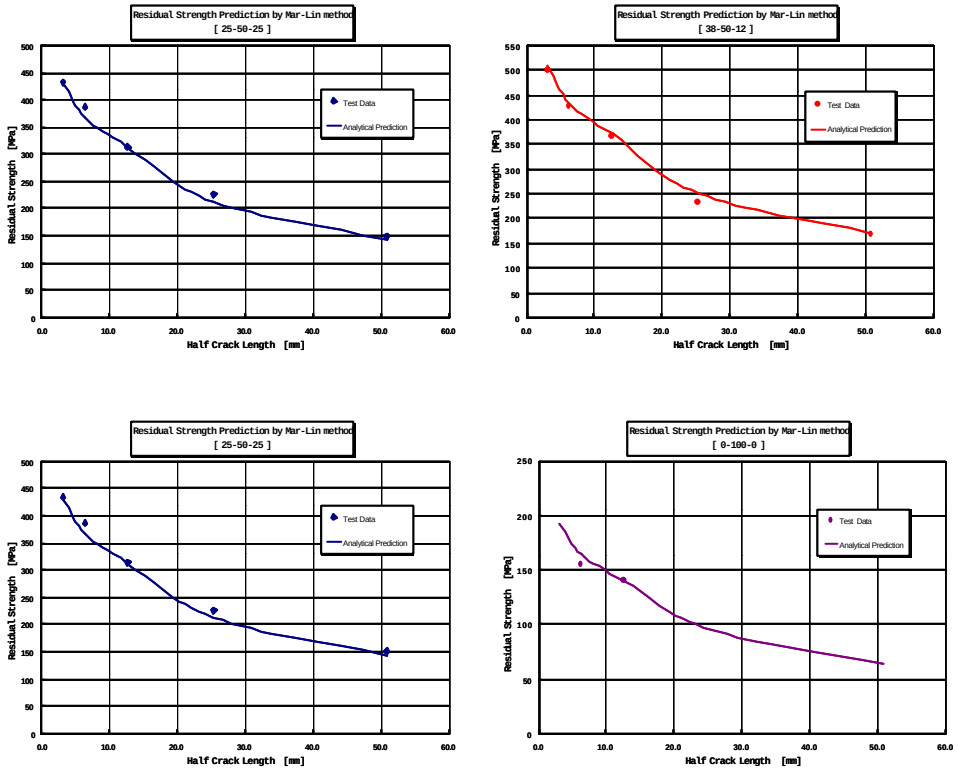

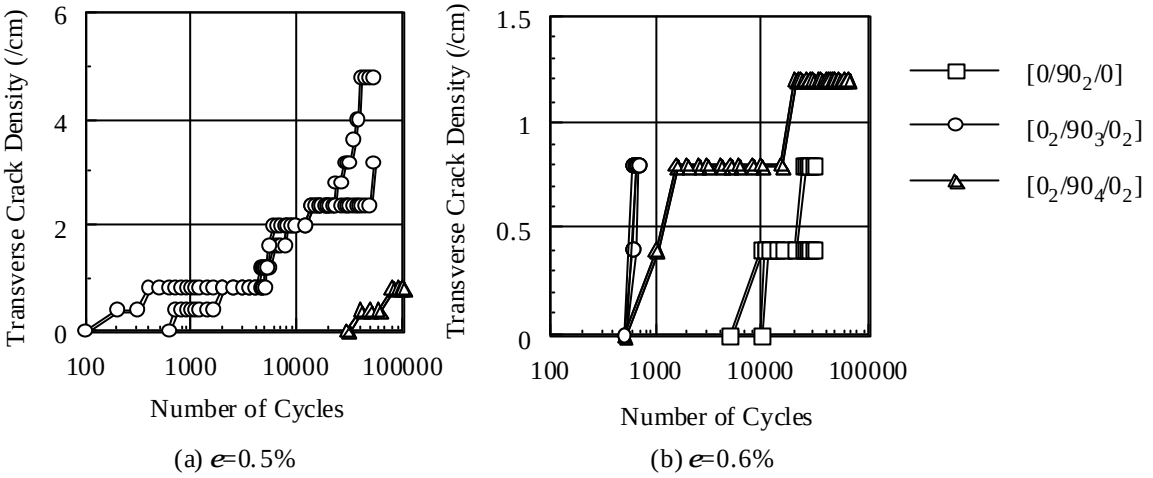

Figure 12.12 Transverse crack density as a function of number of cycles (*e*: the laminate strain corresponding to the maximum cyclic laminate stress)

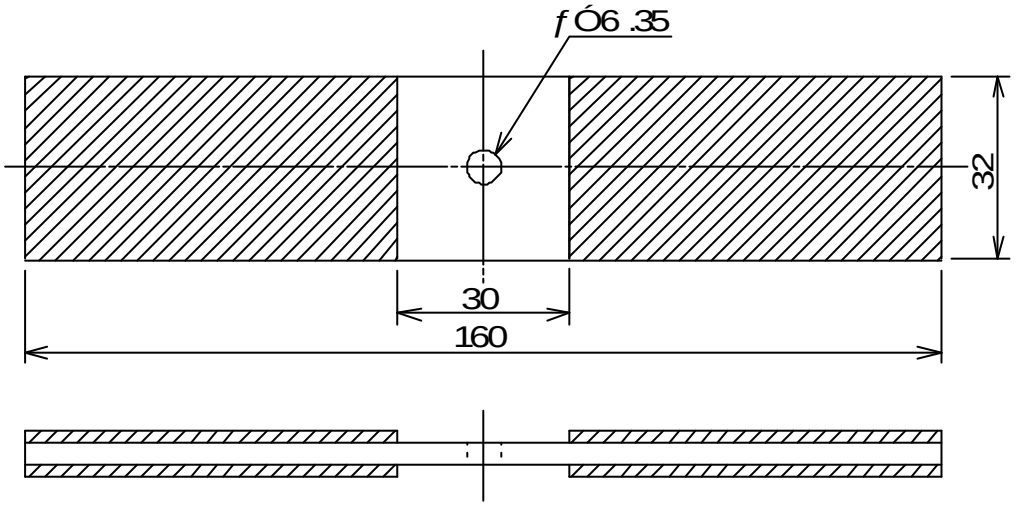

Figure 12.13 Specimen configuration stacking sequence, 32plies (45/0/-45/90)4s

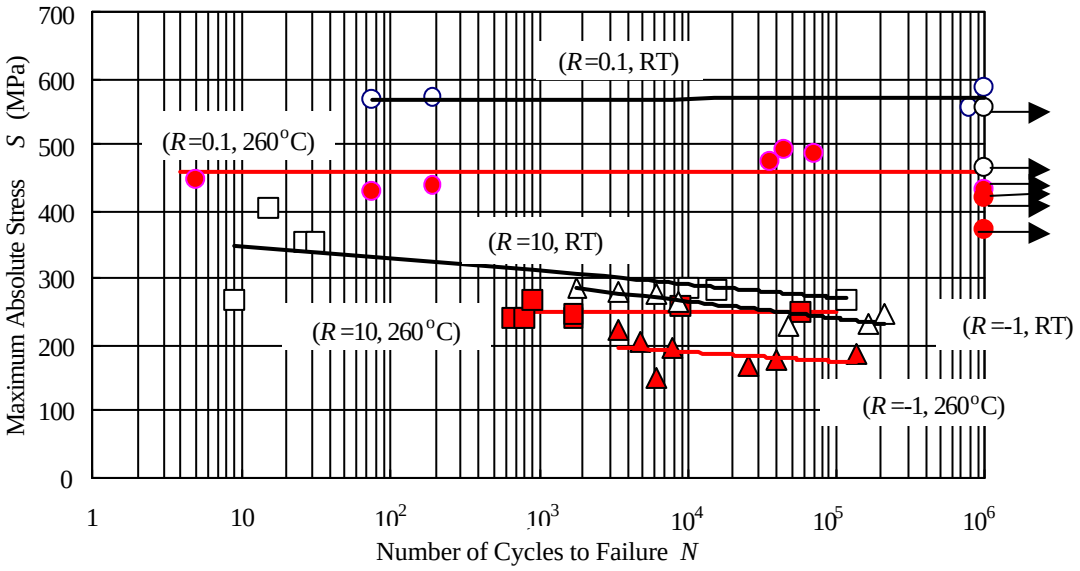

Figure 12.14 S-N relationship of open-hole specimens of T800H/PMR-15 carbon/polyimide composite for three stress ratios at room temperature (RT) and 260°C

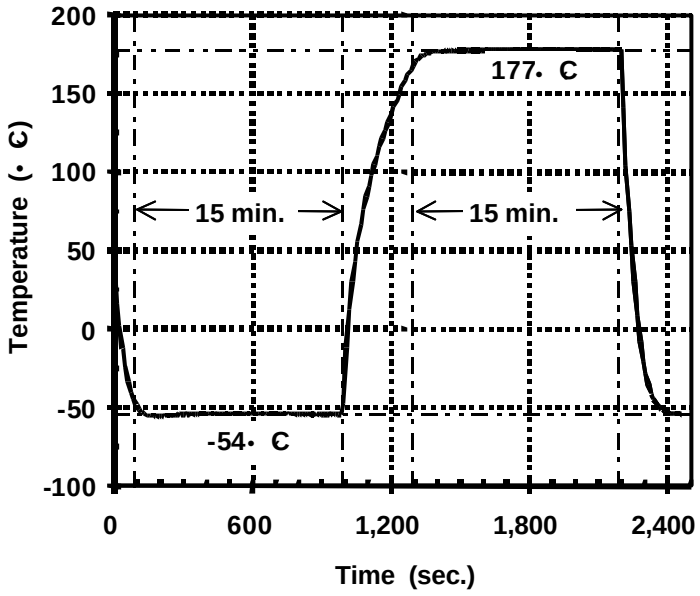

Figure 12.15 Thermal cycle measured in a specimen of the same size as that used for micro-crack observation

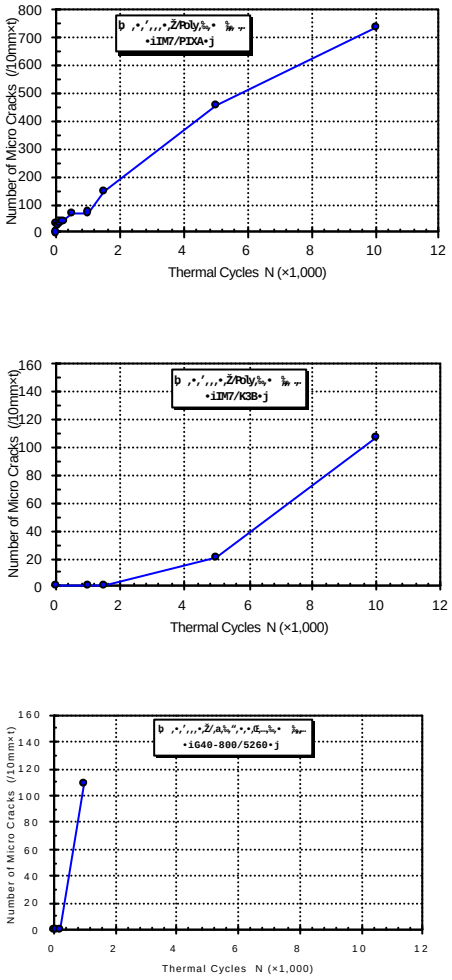

Figure 12.16 Number of microcracks initiated in the sectional area of 10mm thickness as a function of thermal cycles.

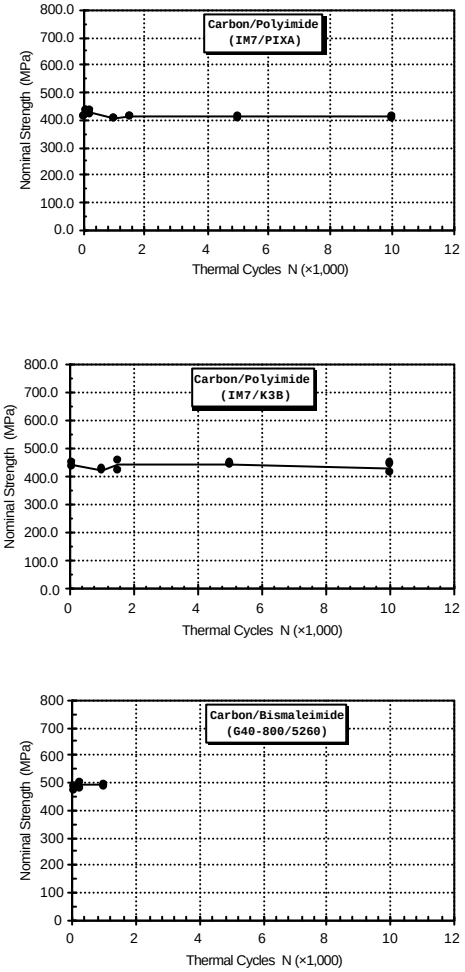

Figure 12.17 Open-hole compressive strength at room temperature before and after thermal cycles.

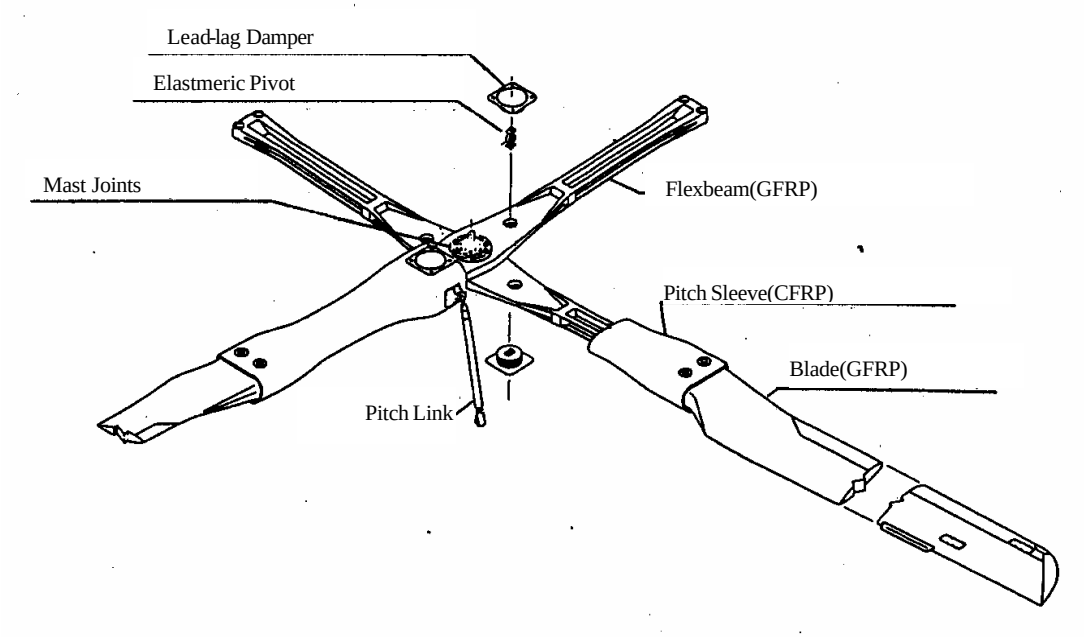

Figure 12.19 Demonstration Flight with Fuji Bearingless Rotor

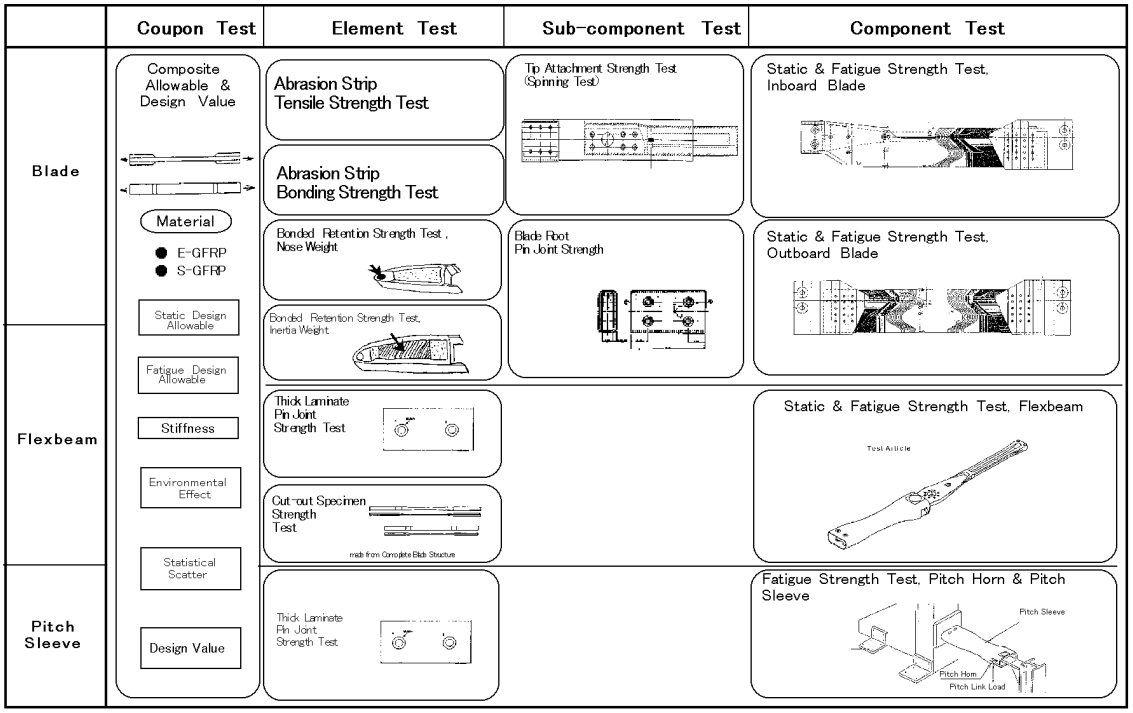

Figure 12.20 Building Block Approach

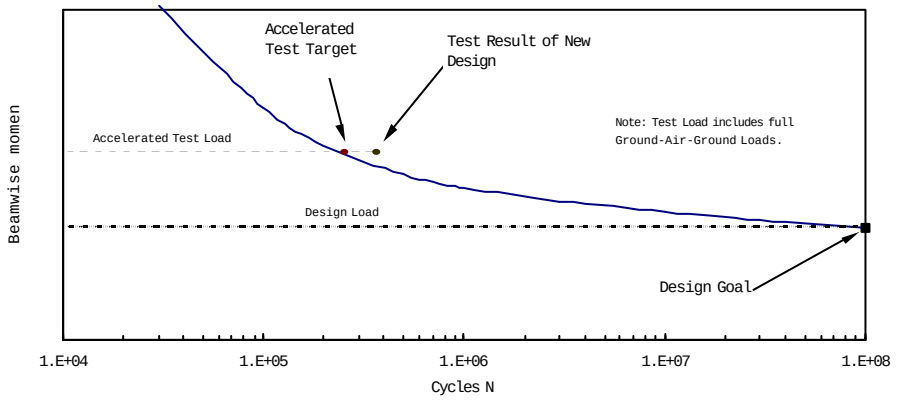

Figure 12.21 Fatigue Test Results of Flexbeam

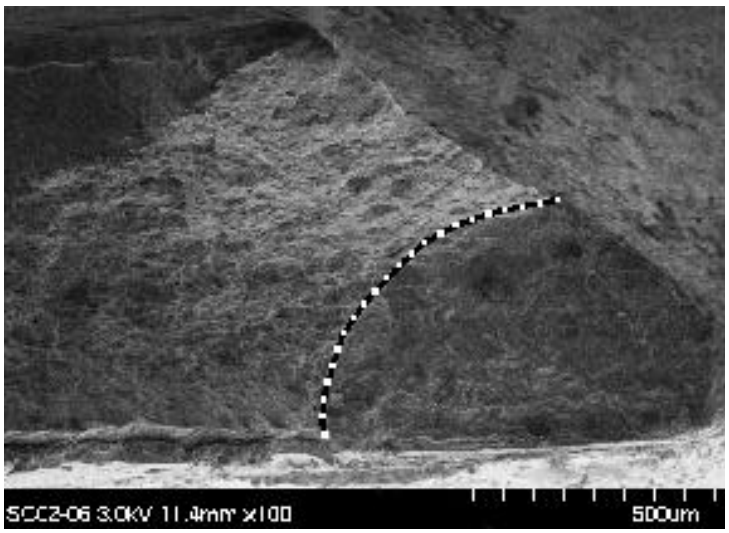

Figure 12.22 Typical corner crack from countersunk rivet hole

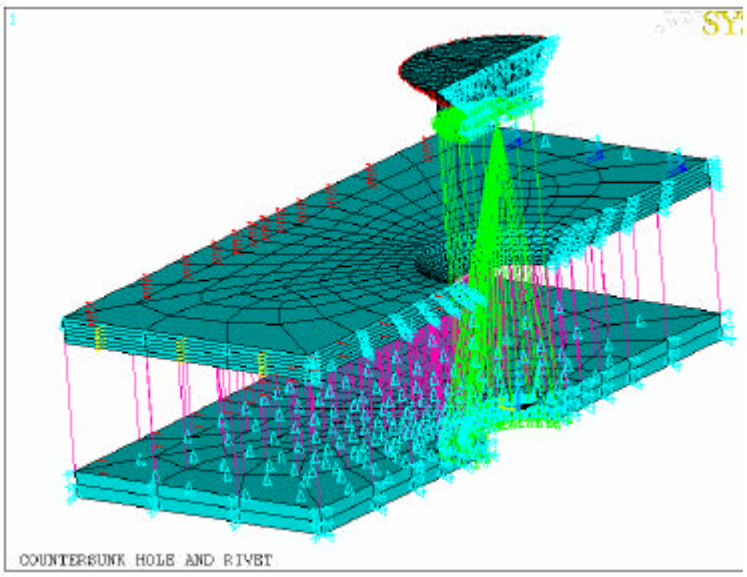

Figure 12.23 FEM model used for analysis (countersunk hole and rivet)

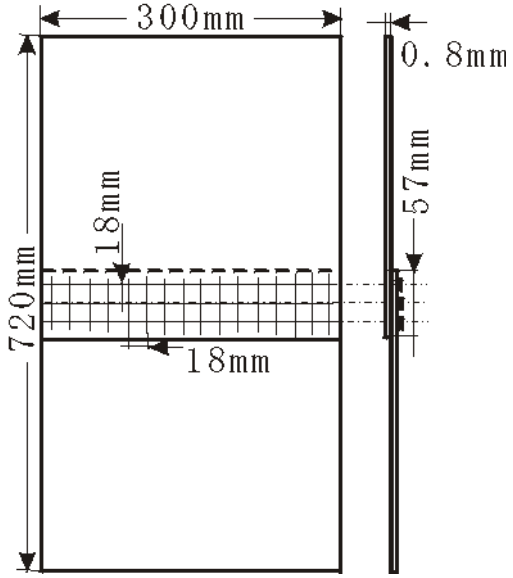

Fig. 12.24 Geometry of specimen

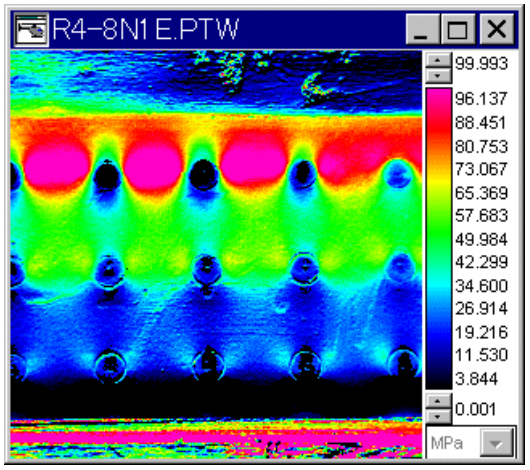

Fig.12.25 Stress distribution at fastener

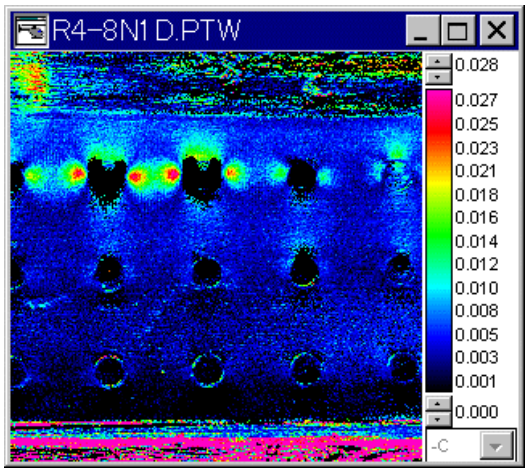

Fig. 12.26 Dissipated energy image at fastener

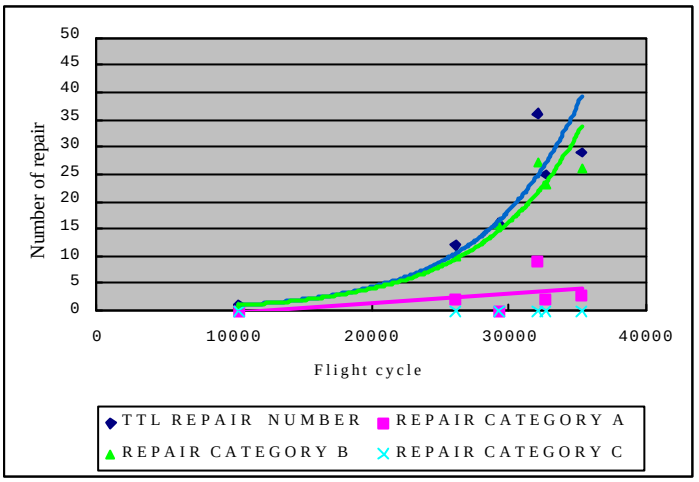

Figure 12.27 Flight cycle vs. Number of doubler

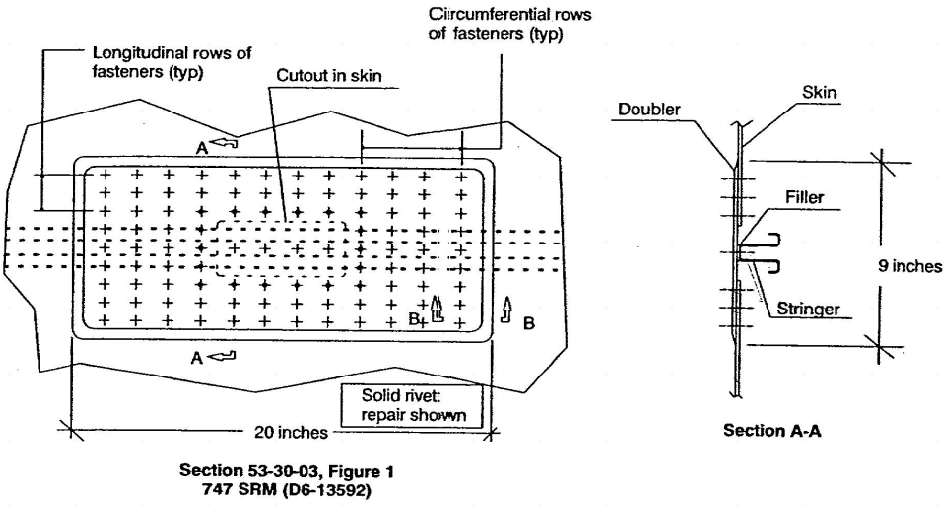

Geometric location: B.S 960 – 980, Stringer 40
Repair dimension: 20 inch X 9 inch X 0.071 inch thickness.
This doubler exceeds 12 inchs in the longitudal direction, then categorized as “B”.

Figure 12.28 Example of category B repair

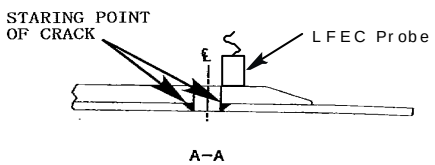

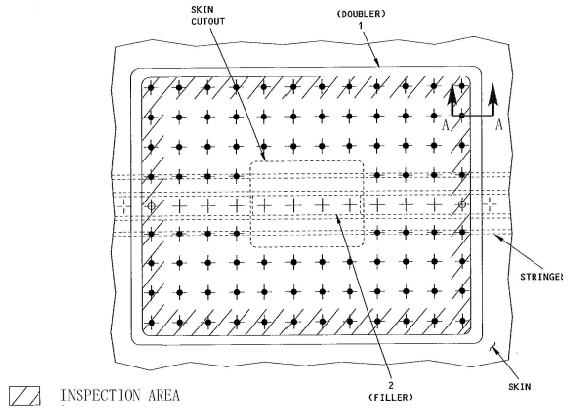

Figure 12.29 Example of Inspection

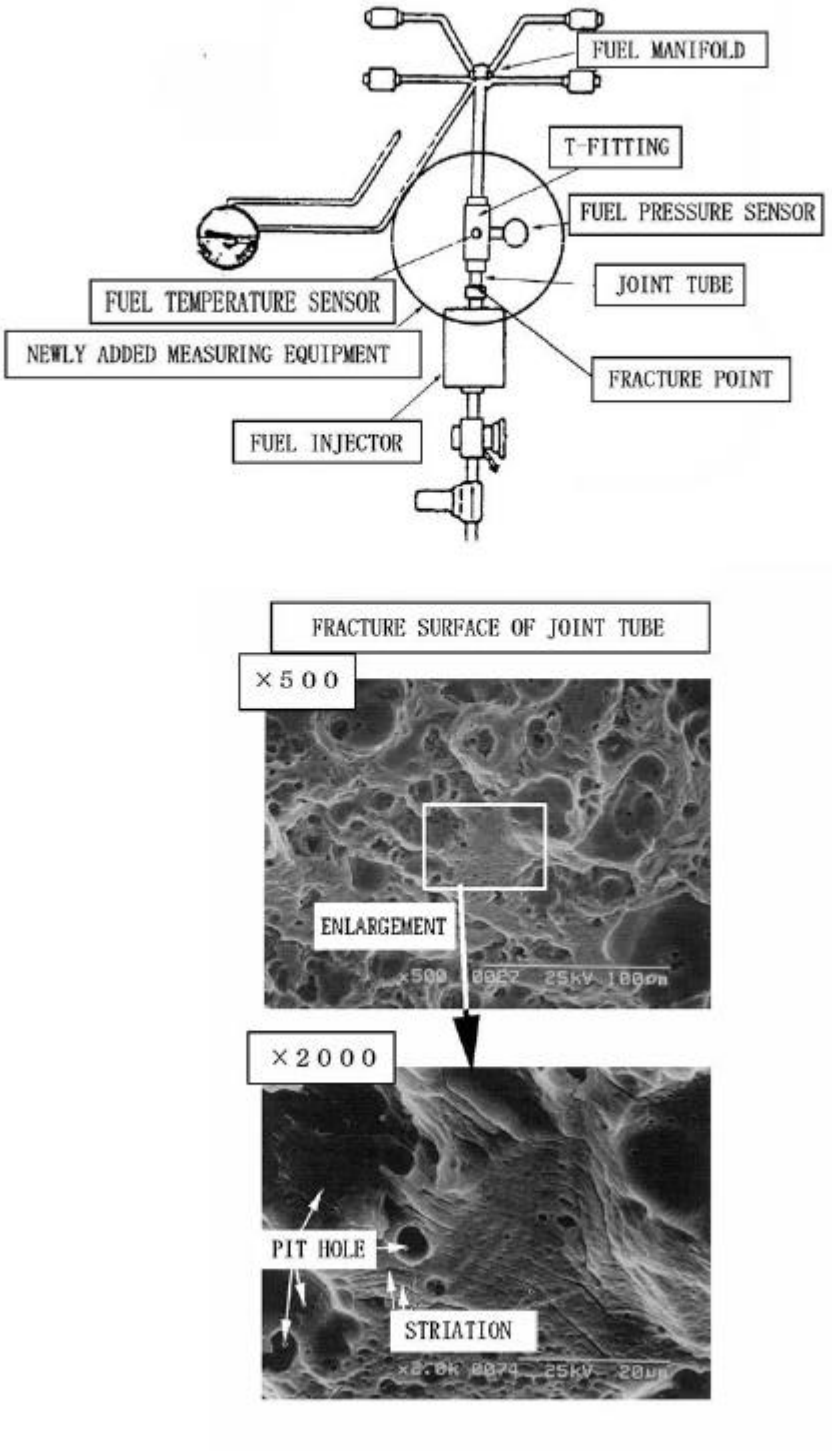

Figure 12.30 Fuel pipe failed by fatigue

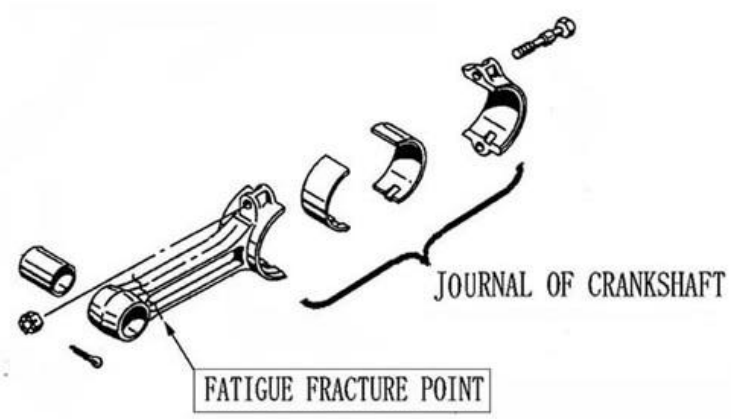

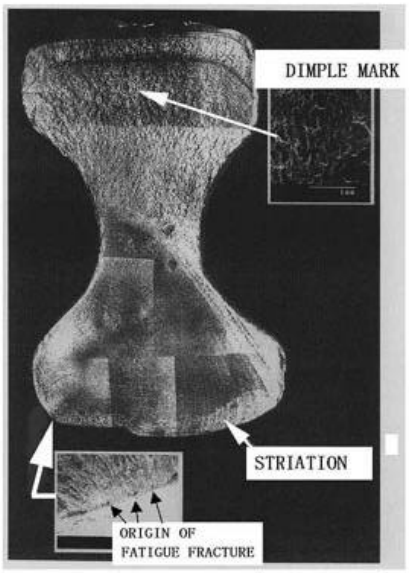

Figure 12.31 Engine connecting rod failed by fatigue